Hindawi
Journal of Nanomaterials
Volume 2019, Article ID 9035297, 11 pages
https://doi.org/10.1155/2019/9035297

Research Article

Polyethylene/Graphene Nanoplatelet Nanocomposite-Based Insulating Materials for Effective Reduction of Space Charge Accumulation in High-Voltage Direct-Current Cables

Ji Sun Park,[1] **Young Sun Kim**,[1] **Hyun-Jung Jung**,[2] **Daseul Park**,[1] **Jee Young Yoo**,[1] **Jin Ho Nam**,[2] **and Yoon Jin Kim**[1]

[1]*Nano Materials & Components Research Center, Korea Electronics Technology Institute (KETI), Seongnam 13509, Republic of Korea*
[2]*Reliability Research Group, LS Cable and System Ltd., Gunpo 15845, Republic of Korea*

Correspondence should be addressed to Jin Ho Nam; Jin-Ho.Nam@lscns.com and Yoon Jin Kim; yj.kim@keti.re.kr

Received 27 September 2018; Accepted 11 February 2019; Published 24 March 2019

Academic Editor: Ilaria Armentano

We have demonstrated a straightforward hydrophobic surface modification of graphene nanoplatelets (GNPs) through a defect-healing process to fabricate well-dispersed insulating low-density polyethylene (LDPE)/GNP nanocomposites and have confirmed their effective suppression of space charge accumulation. Without any organic modifiers, GNPs containing oxygen-based functional groups at the edges were successfully reduced at optimal high-temperature defect-healing condition and modified to have hydrophobic surface properties similar to those of the LDPE matrix. The degree of dispersion and the reproducibility of the mechanically melt-mixed LDPE/GNP nanocomposites were immediately analyzed by thickness-normalized optical absorption measurement. In the LDPE matrix, below the percolation threshold concentration, well-dispersed GNP fillers effectively acted as trapping sites under high electric fields, resulting in the successful suppression of packet-like space charge accumulation (field enhancement factor = 1.04 @ 0.1 wt% LDPE/GNP nanocomposite).

1. Introduction

Because of the surge in energy demand and the rapid development of renewable energy, there is a growing demand for high-voltage direct-current (HVDC) technology to achieve efficient electric power transmission between power generation and power consumption [1–4]. Unlike high-voltage alternating-current (HVAC) cables, charges injected from conducting and semiconducting layers in HVDC cables easily accumulate within the insulating layer, resulting in space charges and causing electric filed distortion and electrical breakdown [5, 6]. Polyethylene, including low-density polyethylene (LDPE), high-density polyethylene (HDPE), and cross-linked polyethylene (XLPE), is a typical insulator used in high-voltage cables [7, 8]. Among the different types of polyethylene, high heat-resistant XLPE is the most widely used insulator owing to its extremely low electrical conductivity, low space charge accumulation, high electrical strength (up to 640 kV), and endurance in electric fields [2, 3]. However, because XLPE is generally made of a mixture of LDPE, organic peroxide, and additives, space charges easily accumulate in the insulating layer of the DC cable when byproducts (or contaminants) are formed during the manufacturing process [9, 10].

To suppress the accumulation of space charges in the insulating layer of a DC cable, many studies have been conducted to add nanofillers with a high dielectric constant (κ) to the polyethylene matrix. Inorganic nanoparticles ($\kappa = 6\sim10$, MgO, SiO_2, Al_2O_3, TiO_2, ZnO, etc.) [11–15] and nanocarbons ($\kappa = 10\sim15$, carbon black, graphene, etc.) [16–18] have mainly been studied as nanofillers acting as charge trapping sites. Such nanofillers are known to provide

charge traps in the polymer matrix that reduce the mobility of charged carriers, including electrons, holes, and polar species. There are various trapping mechanisms such as the bipolar charge-transport model [19], trapping potential model [20], and multicore model [21]; however, according to the trapping potential model of Takada et al., when a high electric field is applied to an LDPE/nanofiller composite, dipoles are induced by dielectric filler and form an electrical potential well, trapping space charges therein. Highly conductive nanocarbons also enable the effective suppression of space charge accumulation by forming deeper potential wells than those of insulating inorganic nanoparticles; however, careful selection of filler size and loading content is required to avoid short-circuit and DC breakdown.

Thus, for nanocarbons to be introduced as a nanofiller that effectively reduces the space charges formed in the polyethylene matrix, a homogeneous dispersion is highly crucial. An inhomogeneous distribution of aggregated nanofillers will maximize the effect of electric field concentration and cause electrical breakdown [11]. Since polyethylene, as a base polymer, is composed of hydrocarbons showing a hydrophobic property, it is advantageous for the nanofiller to have a polyethylene-like surface in order to achieve uniform dispersibility. Hydrophobic surface modification is generally accomplished through covalent or noncovalent bonding between functional groups of nanocarbon and the organic modifier (silane, fatty acid/amine, etc.) [22, 23]. However, when a small amount of residual organic modifiers exists in the insulating layer of the DC cable, it may act as a contaminant and reduce the DC-breakdown threshold-voltage [24].

In this study, we investigated LDPE/graphene nanoplatelet (GNP) insulating nanocomposite for the suppression of space charge accumulation in the insulating layer of a HVDC power cable. For an effective dispersion of GNP fillers in the LDPE matrix, oxygen content on the GNP surfaces was finely tuned through a high-temperature (900°C) defect-healing process and the surfaces readily changed to hydrophobic under optimal annealing condition. The surface of the GNPs was successfully modified without the use of organic modifiers, and the quantitative dispersibility in the LDPE matrix was immediately analyzed via visible-light absorption-based optical measurement. The LDPE nanocomposite with defect-healed hydrophobic GNP fillers effectively suppressed the formation of packet-like space charges.

2. Materials and Methods

2.1. Materials. GNP powder was purchased from XG Science (C-750 grade, U.S.A.) and LDPE pellet was kindly supplied by LG Chem. Ltd. (Republic of Korea). All other chemicals used in this study were purchased from Sigma-Aldrich (U.S.A.).

2.2. Preparation of LDPE Nanocomposites Containing Defect-Healed GNP Fillers. First, GNP powders were thermally treated at 900°C for 2 hours under Ar/H_2 (200/160 sccm) atmosphere. Thermally treated GNPs with different filler contents of 0.01, 0.03, 0.05, and 0.1 wt% were mechanically mixed with LDPE pellets for 5 minutes in a resonant acoustic mixer (RAM). GNP-coated LDPE pellets were melt-mixed at 160°C for 30 minutes using a HAAKE internal mixer. The mixed compound was hot-pressed in a mold at 160°C under 20 MPa for 30 minutes and cooled to room temperature to prepare the sample sheet.

2.3. Space Charge and Volume Resistivity Measurement. Space charge distribution was measured by pulsed electroacoustic (PEA) method under DC electric field of 50 kV/mm for 60 minutes. A positive DC voltage was applied to the sample using semiconducting layer (upper) and aluminum plate (lower grounded) electrode system. The upper electrode diameter was 40 mm and sample thickness was 150 ~ 200 μm. Charging and discharging tests were carried out for 60 minutes and 5 minutes, respectively.

Volume resistivity of sample with thickness of 150 ~ 200 μm was measured at room temperature (25°C), 50°C, and 70°C. The measurement was performed using a three-electrode (measuring electrode, counter electrode, and guard electrode) system; the diameter of measuring electrode was 24 mm. The charging current in the electric field of 10 kV and 20 kV was measured by electrometer for 7,200 seconds. Then, volume resistivity was calculated by the following equation [17]:

$$\rho = \frac{E}{I} \bullet \frac{\pi d^2}{4}, \tag{1}$$

where ρ is the volume resistivity. I is the mean value of the charging current during the last 30 seconds. E is the strength of the electric field and d is the diameter of the measuring electrode.

2.4. Characterization. The surface morphology and cross section of the sample were investigated by field emission scanning electron microscope (FE-SEM, Hitachi S-4800, accelerating voltage: 15 kV) and high-resolution transmission electron microscope (HR-TEM, JEM-2100F, JEOL). The microscale distribution of fillers in the LDPE matrix was observed via optical microscope (OM, Hirox KH-8700). The absorbance of the sample was measured by ultraviolet-visible (UV-VIS, Jasco, V530) spectroscopy. The elemental contents (C and O) and chemical functional groups of the GNP powders were analyzed using X-ray photoelectron spectroscopy (XPS, K-Alpha, Thermo Electron).

3. Results and Discussion

Figures 1(a) and 1(b) show the images of LDPE pellets and GNP powders used in this study. In order to prepare the LDPE/GNP insulating nanocomposite, LDPE pellets and GNP powders were mixed in a dry state using a resonant acoustic mixer (RAM) (Figure 1(c)). By controlling the vibration through acceleration and frequency in the RAM, GNP particles were uniformly embedded (or coated) on the LDPE pellet surfaces (Figure 1(d)). Furthermore, aggregated GNP particles above several tens of micrometers were effectively pulverized by strong collisions between particles in the RAM mixing step [25]. The surface morphologies of GNP-

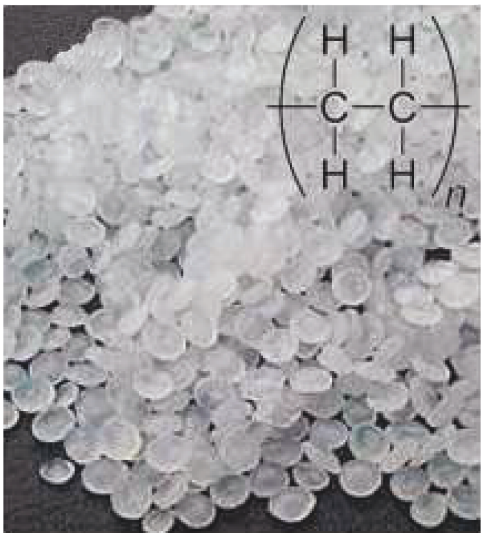

(a)

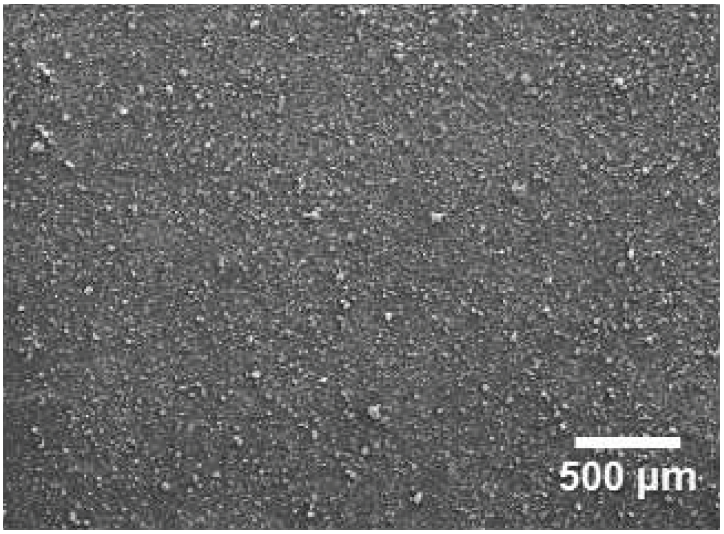

(b)

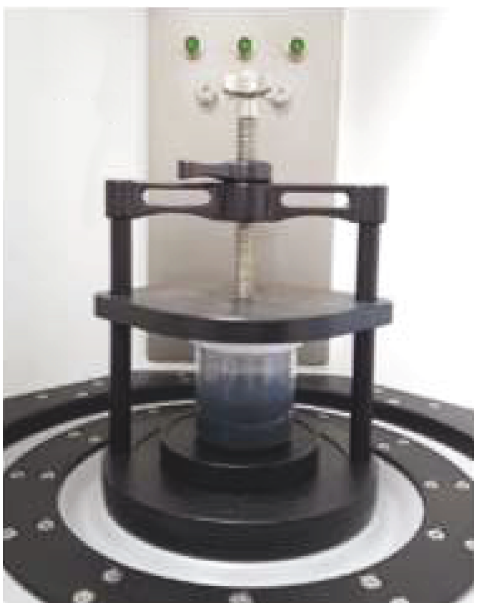

(c)

(d)

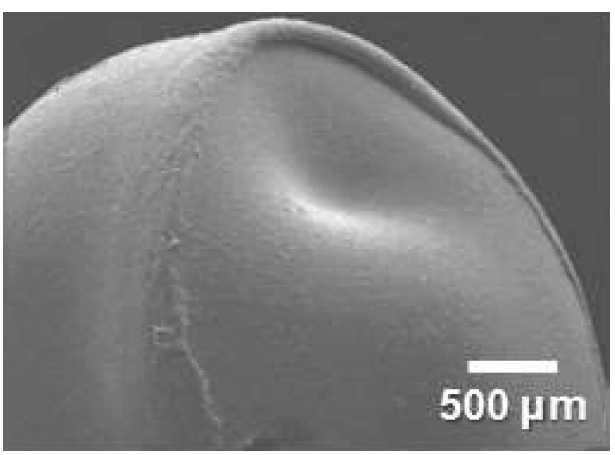

(e)

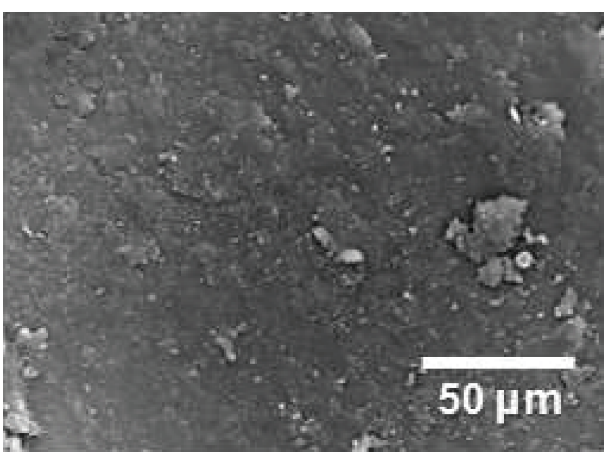

(f)

Figure 1: Continued.

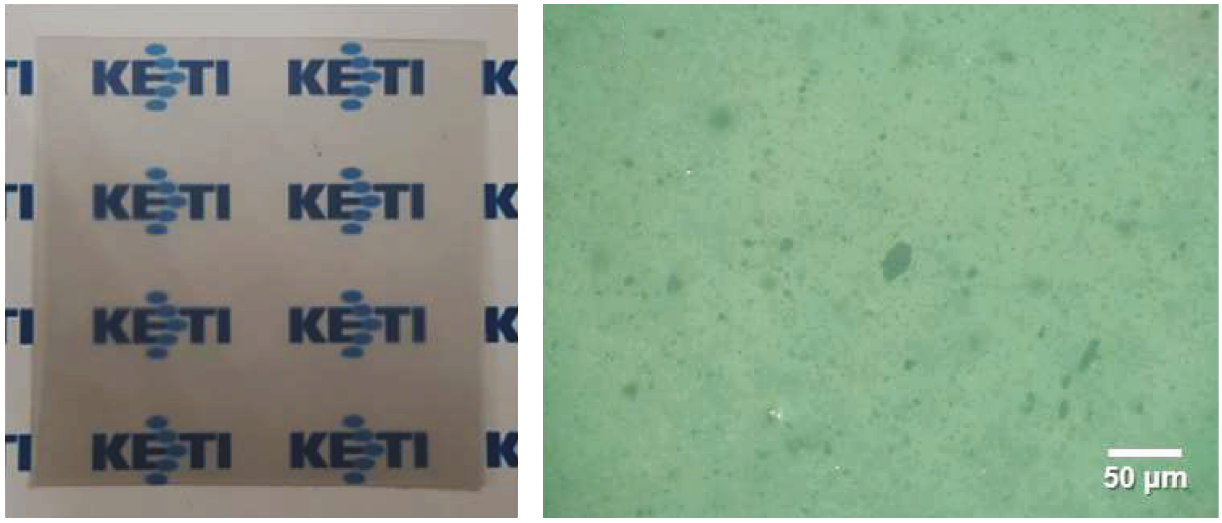

(g) (h)

Figure 1: Photographs of (a) LDPE pellets, (b) GNP powders, and (c) RAM equipment employed for mixing them. (d) Photograph of GNP-coated LDPE pellets. SEM image of (e) GNP-coated LDPE pellet surface and (f) higher magnification SEM image. (g) Photograph of LDPE/GNP nanocomposite with 0.1 wt% pristine GNP filler content and (h) optical microscope image of same.

coated LDPE pellets are shown in Figures 1(e) and 1(f). Through melt-mixing process in the internal mixer, GNP-coated LDPE pellets were mechanically mixed at 160°C for 30 minutes; finally, LDPE/GNP insulating nanocomposite was fabricated. Figure 1(g) shows a photograph of the LDPE/GNP nanocomposite containing 0.1 wt% pristine GNP fillers; the distribution of the fillers within the LDPE matrix was observed through an optical microscope (OM) (Figure 1(h)). Since the pristine GNPs (as received) had an oxygen content of approximately 13%, filler dispersion was not properly accomplished due to the surface energy mismatch between hydrophobic LDPE matrix and GNP fillers, resulting in large amounts of GNP aggregate.

To improve the dispersibility of the GNP fillers in the LDPE matrix, hydrophobic surface modification of GNPs was carried out by defect-healing process. A schematic of the experimental defect-healing process is presented in Figure 2(a). Defect healing of GNP powders was performed at 900~1,000°C under Ar/H_2 (200/160 sccm) atmosphere. During the process, oxygen functional groups (-OH, -COOH, and C-O-C), mainly attached on the edges of the GNPs, were rapidly removed in the form of CO or CO_2 gases. Figure 2(b) shows carbon (C) and oxygen (O) contents according to the reduction time of GNPs at 900°C and 1000°C, respectively. The elemental content of each sample was analyzed by XPS measurement. The initial C and O contents and C/O ratio of pristine GNPs were 87.02%, 12.98%, and 6.7, respectively. Comparing the degrees of reduction at 900°C and 1000°C under identical reduction time (@ 120 min.), C/O ratio (24.6) at 900°C was found to be 1.8 times higher than C/O ratio at 1000°C (13.6). At a fixed reduction temperature of 900°C, C/O ratio gradually increased until reduction time of 120 minutes; however, when the reduction time was longer than that, C/O ratio decreased (inset of Figure 2(b)). Thus, we selected optimum defect-healing temperature and time of 900°C and 120 minutes, respectively, to minimize the O content of GNPs; the O content at that condition was 3.91% (we denote the defect-healed GNP as GNP-T). In order to confirm the degree of surface modification of GNPs with the naked eye, solvent test was performed, with results shown in Figure 2(c). First, the same amounts of pristine GNP and GNP-T powder were forcibly dissolved in DI water; then, xylene was added and the mixture was vigorously stirred. The resulting pristine GNP was distributed both in hydrophilic DI water and hydrophobic xylene phases, whereas GNP-T was predominantly distributed in a hydrophobic xylene phase. This is attributed to the surface of GNP-T, which is effectively modified to be hydrophobic without any organic modifiers.

Figure 3 shows high-resolution XPS spectra of C 1s peak of the pristine GNP and GNP-T. As shown in Figure 3(a), pristine GNP mainly showed peaks including graphitic C-C (284.9 eV)/C=C (284.5 eV), C-OH (285.5 eV), C-O-C (286.9 eV), and O=C-OH (289.4 eV) [26]. However, for GNP-T, the intensities of the graphitic C-C/C=C peaks were stronger than those of the pristine GNP; the peak intensities associated with oxygen functional groups (C-OH, C-O-C, and O=C-OH) significantly decreased. It is worth noting that simple heat treatment of the GNPs is sufficient to lower the oxygen content and alter the surface property, which is advantageous for actual mass production.

Figure 4 provides OM images of the LDPE/GNP insulating nanocomposites, including pristine GNP (Figure 4(a)–4(d)) and GNP-T fillers (Figure 4(e)–4(h)) with filler contents of 0.01, 0.03, 0.05, and 0.1 wt%. Each composite sheet was prepared by hot-press molding (insets of Figure 4). To evaluate the microscale dispersibility of the GNP fillers in the LDPE matrix, a small piece of composite sheet was inserted between transparent slide glasses and subsequently hot-pressed to fabricate a visually flat sample for OM observation. At the same filler content, GNP-T fillers were more homogeneously dispersed than pristine GNP fillers, without severe aggregation,

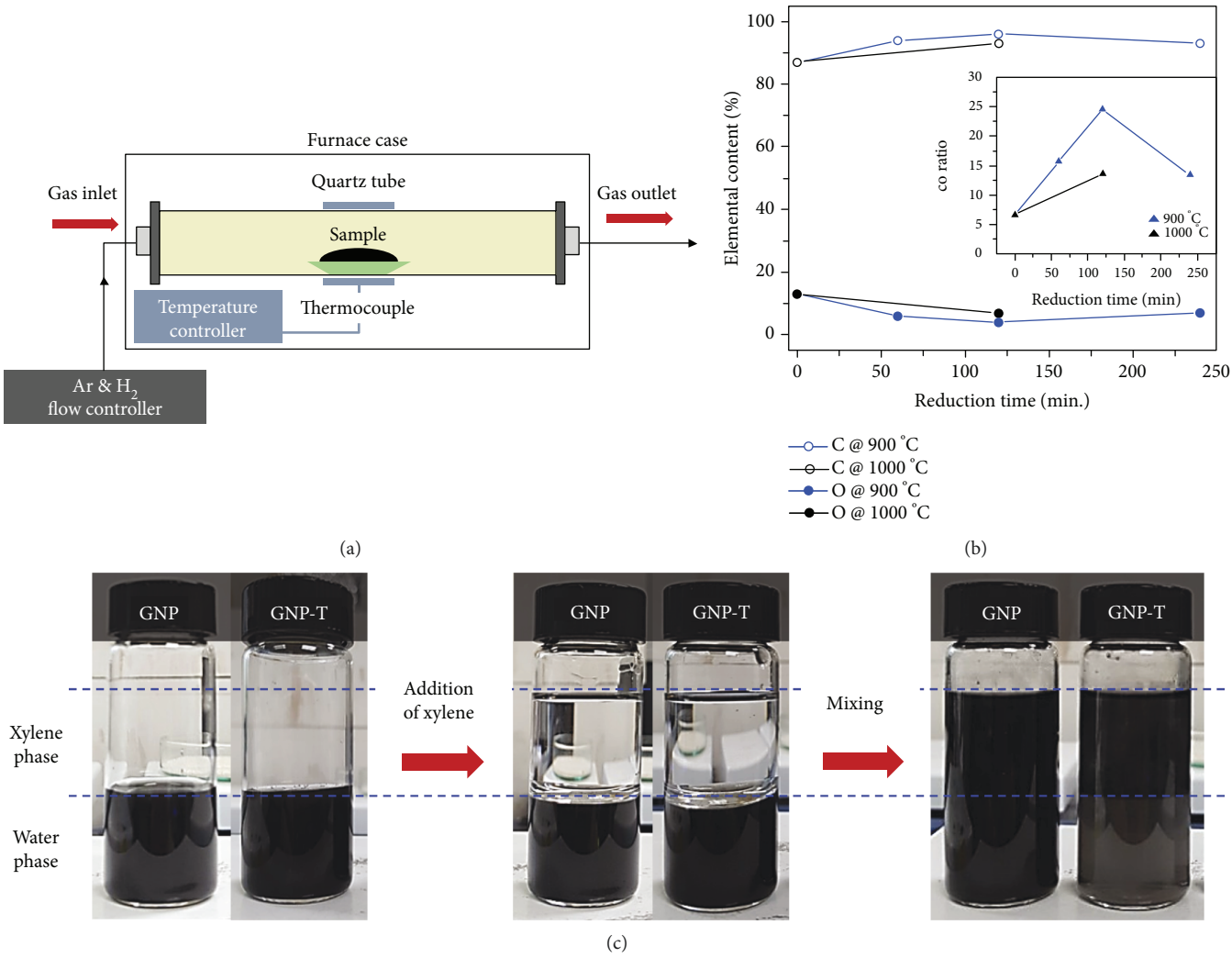

FIGURE 2: (a) Schematic of defect-healing process for GNP powders. (b) Plot of C and O contents of GNPs at different defect-healing temperatures and times (inset: plot of C/O ratio of GNPs at different defect-healing temperatures and times). (c) Photographs of GNP-T fillers transferred from water phase to xylene phase by surface modification via defect-healing process.

whereas pristine GNPs exhibited noticeable aggregations of tens of micrometers in lateral size. This is due to the surface energy mismatch between pristine GNP and LDPE matrix, as shown in Figures 2(b) and 3(a). To analyze the OM images accurately, the sizes of the maximum GNP-T filler aggregates within the LDPE matrix were measured using a commercial image processing tool (Figure S1). Compared to the pristine GNP fillers, it was found that the aggregate size of the GNP-T fillers was reduced by half in the entire filler concentration range and the maximum aggregate size was under 10 μm.

In order to quantify the dispersibility of the GNP fillers in the LDPE matrix, the degree of dispersion of the nanocomposite was analyzed by applying the Beer-Lambert law [27, 28]. According to the Beer-Lambert law ($A = \varepsilon \cdot t \cdot c$), the absorbance ($A$) of the composite is proportional to the effective optical absorption coefficient (ε) at the same filler concentration (c) and composite thickness (t). Since the dispersibility of the composite is enhanced at the same filler concentration and composite thickness, the effective surface area of the fillers capable of absorbing light increases, resulting in high absorbance and high optical absorption coefficient. Figure 5 shows the thickness-normalized absorbance plot of the LDPE/GNP insulating nanocomposites, shown in Figure 4, as a function of the filler (pristine GNP and GNP-T) concentration. The absorbance of the nanocomposite, defined as $A = -\log T$ (T: transmittance), was measured by UV-VIS spectroscopy at 550 nm wavelength; optical absorption coefficient was calculated from the slope of the plot. In the entire concentration range between 0.01 and 0.1 wt%, LDPE/GNP-T nanocomposite presented higher thickness-normalized absorbance than the LDPE/pristine GNP nanocomposite; the slopes of the plots were 18.9 (@ LDPE/pristine GNP nanocomposite) and 25.1 (@ LDPE/GNP-T nanocomposite), respectively. A comparison of these slopes shows that the dispersibility of the LDPE/GNP-T nanocomposite is 33% better than that of the LDPE/pristine GNP nanocomposite.

Figure 6 shows cross-sectional SEM images of the LDPE nanocomposites having pristine GNP (Figure 6(a)) and GNP-T fillers (Figure 6(b)), at 0.1 wt% filler content. Dispersed fillers were marked with yellow arrows; the aggregate

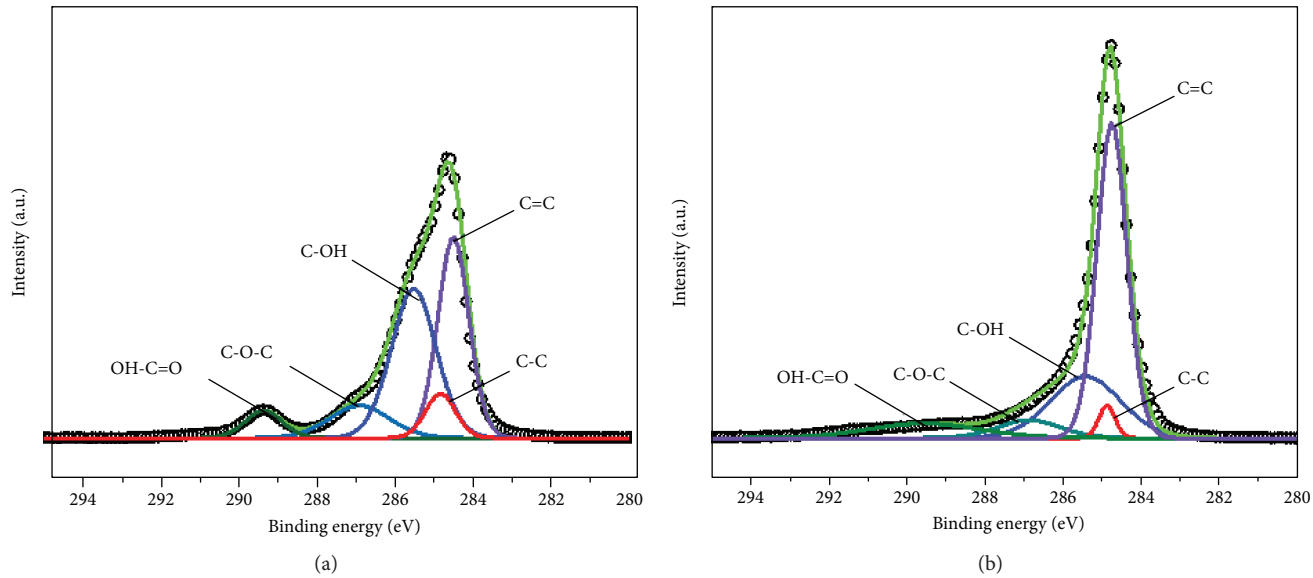

Figure 3: High-resolution XPS spectra of C 1s peaks of (a) pristine GNP (C: 87.02%, O: 12.98%) and (b) GNP-T (C: 96.09%, O: 3.91%) fillers.

size of the GNP-T fillers was obviously reduced after surface modification of pristine GNP fillers through defect-healing process. Furthermore, the effective surface area of GNP-T fillers in the same composite area was greater than that of the pristine GNP fillers owing to the effective dispersion of the fillers in the LDPE matrix, which is consistent with the absorbance results shown in Figure 5. Figure 6(c) provides a TEM image of the LDPE/GNP-T nanocomposite thin film with separately isolated filler morphology.

To investigate the trapping effect of the GNP-T fillers in the LDPE nanocomposite, space charge density was measured using pulsed electroacoustic (PEA) method [29]. Since highly conductive GNP-T fillers can easily form a conductive path at high filler content, space charge distributions of the LDPE/GNP-T nanocomposites with low filler content (under the percolation threshold) of 0.01 wt%-0.1 wt% (Figure 4(e)–4(h)) were only analyzed for 3,600 seconds under DC electric field of 50 kV/mm, with results in Figure 7. Electric field distributions after the application of stress for 3,600 seconds are shown at the bottom of the figure. Figure 7(a) presents the space charge behavior of a neat LDPE sample. As the charging time increased, it can be clearly seen that positive packet-like charges appeared at the anode-LDPE interfaces and moved from anode to cathode. Although the exact mechanism has not been elucidated, the accumulation of space charges is considered to be due to charged carriers in the LDPE matrix, such as byproducts that occur during the polymer synthesis process. As the content of GNP-T fillers in the LDPE matrix increased from 0.01 wt% (Figure 7(b)) to 0.1 wt% (Figure 7(e)), space charges that accumulated in the bulk LDPE nanocomposites moved more slowly than in the neat LDPE matrix and were hardly observed at filler content of 0.1 wt%. It is considered that dipoles induced near the dielectric GNP-T fillers under the high electric field formed a deep potential well, and so homocharges injected near the electrode were effectively trapped there by the high potential barrier to Schottky injection. Thus, space charge accumulation was suppressed, and effective electric field at the electrode-polymer interface was consequently reduced, similar to the case of initially applied electric field [20]. Maximum enhanced electric fields of neat LDPE and LDPE/GNP-T nanocomposites are summarized in Figure S2. The maximum enhanced electric field showed a value of 67 kV/mm inside the neat LDPE sample due to the movement of positive packet-like charges from anode to cathode; field enhancement factor (FEF), which is the ratio of the electric field before and after the accumulation of space charges, was 1.34 (=67 $kVmm^{-1}$/50 $kVmm^{-1}$). However, for the LDPE/GNP-T nanocomposite containing 0.1 wt% filler content, maximum enhanced electric field showed the smallest value of 52 $kVmm^{-1}$ (FEF = 1.04) among the five samples (Figures 7(a)–7(e)) owing to the suppressed space charges.

Figure 8(a) shows the volume resistivity of the LDPE/GNP-T nanocomposites as a function of GNP-T filler content under constant electric fields of 10 kV/mm (@ 25°C, red triangle) and 20 kV/mm (@ 25°C, blue triangle). The volume resistivity of each nanocomposite was determined by averaging the volume resistivity values during the last 30 seconds of the charging time (for 7,200 seconds)-volume resistivity plot. Under an electric field of 10 kV/mm, nanocomposite showed the highest value of $5.55 \times 10^{17}\ \Omega \cdot cm$ at 0.1 wt% filler content, whereas it had values of $3.5 \times 10^{17}\ \Omega \cdot cm$, $2.6 \times 10^{17}\ \Omega \cdot cm$, and $4.0 \times 10^{17}\ \Omega \cdot cm$ for 0.05 wt%, 0.01 wt%, and 0 wt% filler contents, respectively. Despite graphene being a highly conductive material, 0.1 wt% LDPE/GNP-T nanocomposite, which has a filler content far below the percolation threshold, showed higher volume resistivity than neat LDPE. The increase in volume resistivity of the nanocomposite compared to the neat LDPE was greater at an electric field of 20 kV/mm; their volume resistivity values were $1.3 \times 10^{16}\ \Omega \cdot cm$ (@ 0 wt%), $9.4 \times 10^{16}\ \Omega \cdot cm$ (@ 0.01 wt%), $7.4 \times 10^{16}\ \Omega \cdot cm$ (@ 0.05 wt%), and $8.6 \times 10^{16}\ \Omega \cdot cm$ (@ 0.1 wt%). According to a previous study on trap level distribution of insulating

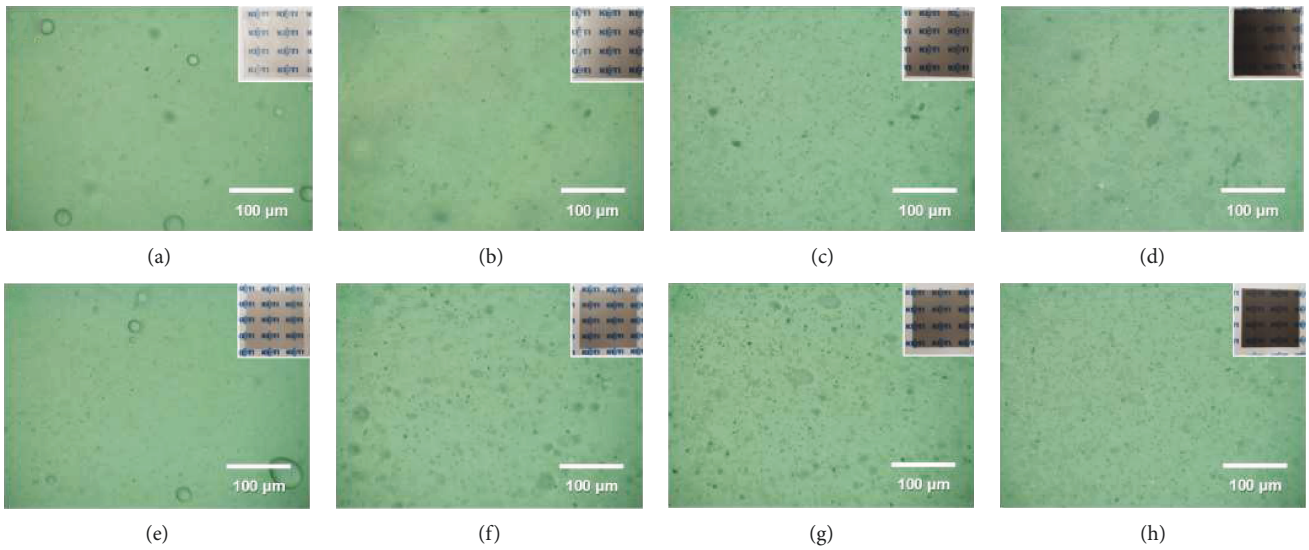

Figure 4: Optical microscope images of LDPE nanocomposites containing pristine GNPs ((a) 0.01 wt%, (b) 0.03 wt%, (c) 0.05 wt%, (d) 0.1 wt%) and GNP-T ((e) 0.01 wt%, (f) 0.03 wt%, (g) 0.05 wt%, (h) 0.1 wt%) fillers (inset: photographs of corresponding LDPE nanocomposites).

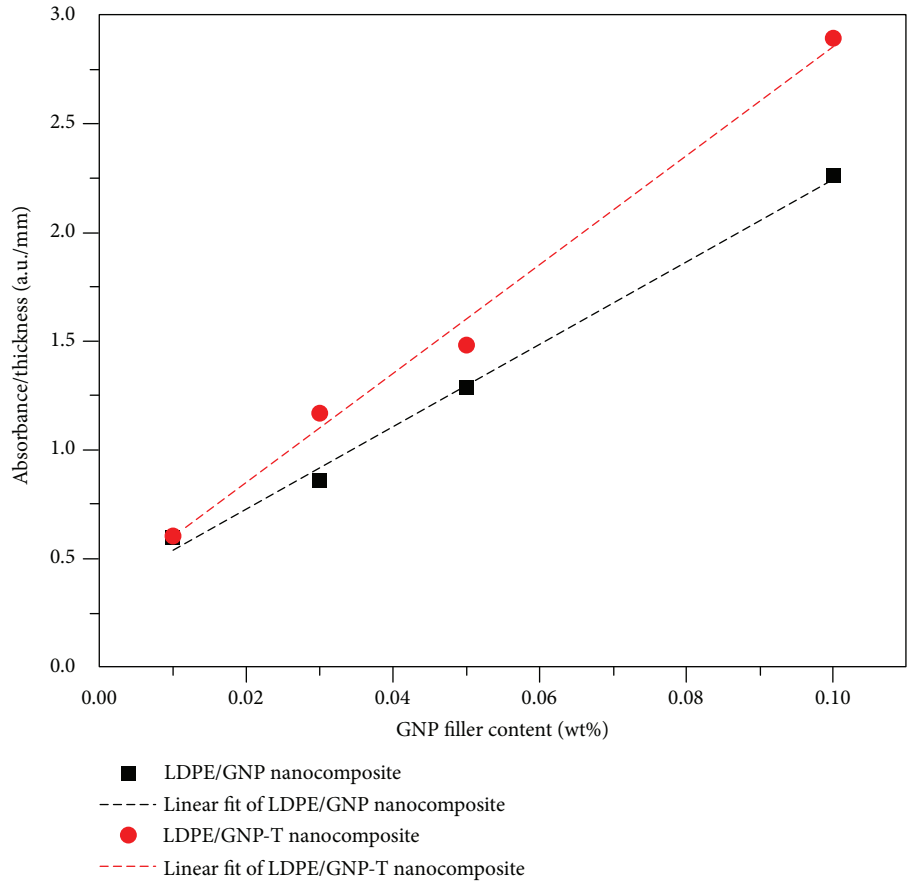

Figure 5: Thickness-normalized absorbance plot of LDPE nanocomposites containing pristine GNP and GNP-T fillers, as a function of filler content.

nanocomposites, the density of deep traps increased up to optimum filler content and then decreased at higher filler content than optimum point. The volume resistivity of the nanocomposites showed the highest value at the filler content with the highest density of deep traps. This attributes that large numbers of deep traps capture holes and electrons and

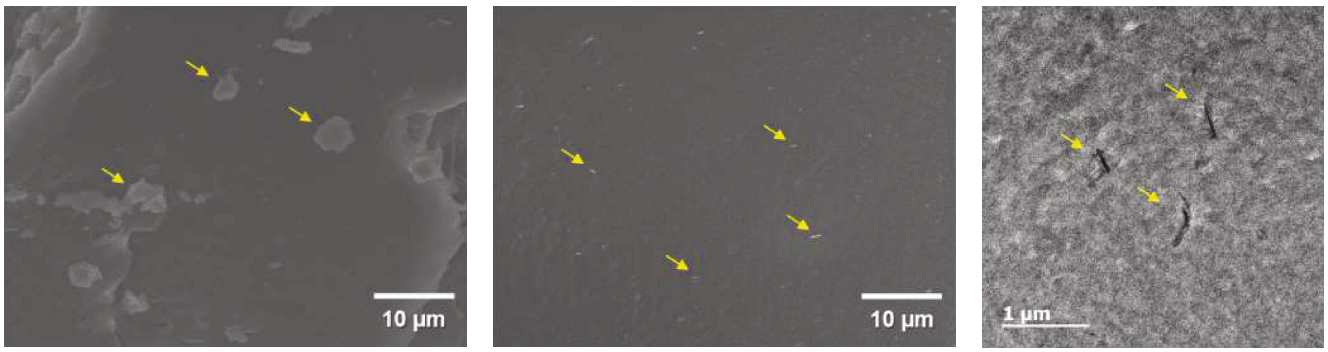

Figure 6: Cross-sectional SEM images of (a) LDPE/pristine GNP nanocomposite and (b) LDPE/GNP-T nanocomposite with 0.1 wt% filler content. (c) TEM image of LDPE/GNP-T nanocomposite with 0.1 wt% filler content.

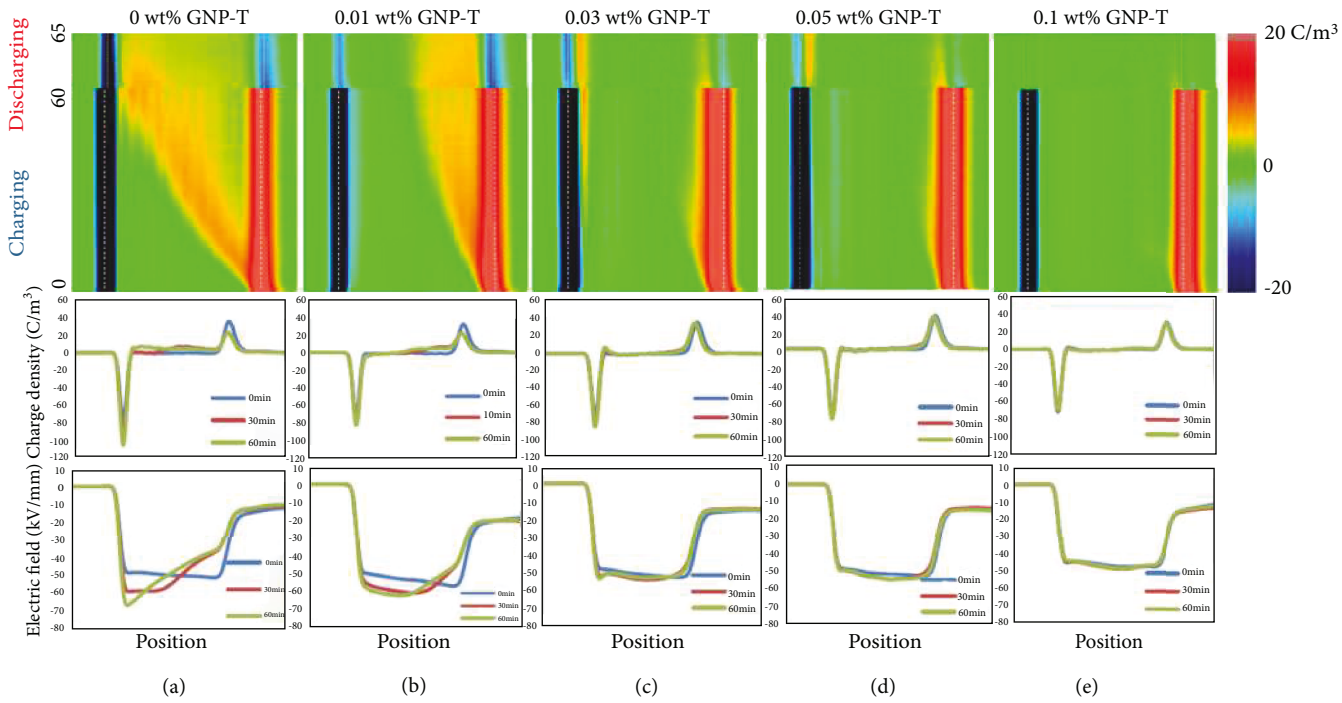

Figure 7: Space charge behaviors of neat LDPE and LDPE/GNP-T nanocomposites under DC electric field of 50 kV/mm, measured by PEA method, and electric field distribution after application of stress for 3,600 seconds. (a) Neat LDPE, (b) 0.01 wt%, (c) 0.03 wt%, (d) 0.05 wt%, and (e) 0.1 wt% GNP-T containing LDPE nanocomposites.

increase the average hopping distance for the charged carriers, thus suppressing the transport of charged carriers [17]. From these results, it is believed that dielectric GNP-T fillers (below the content of percolation threshold) can effectively capture charged carriers injected from the electrode, resulting in an increase in the volume resistivity of the nanocomposite rather than neat LDPE. This is consistent with the result of space charge measurement in Figure 7.

Since high voltage (V) levels inevitably cause considerable electrical stress and temperature rise ($\triangle T \propto V^2/\rho$), which may result in electrical breakdown in the HVDC insulating material, ultrahigh volume resistivity (ρ) is required to prevent the risk of thermal runway and electrical failure [30].

In order to observe the temperature and electric field dependence of the volume resistivity, additional volume resistivity measurement was performed at different temperatures (25, 50, and 70°C) and electric field (10, 20 kV/mm) conditions for the LDPE/GNP-T nanocomposites having filler contents of 0 wt% (neat LDPE, hollow triangle) and 0.1 wt% (triangle) (Figure 8(b)). As the temperature increased from 25°C to 70°C at 10 kV/mm, the volume resistivity of the 0.1 wt% LDPE/GNP-T nanocomposite dropped from $5.5 \times 10^{17}\ \Omega \cdot$ cm to $8.7 \times 10^{15}\ \Omega \cdot$ cm; it was further decreased to values of $8.6 \times 10^{16}\ \Omega \cdot$ cm (@ 25°C) and $9.1 \times 10^{14}\ \Omega \cdot$ cm (@ 70°C) at 20 kV/mm. However, in the case of neat LDPE, as the temperature increased under the same electric field condition,

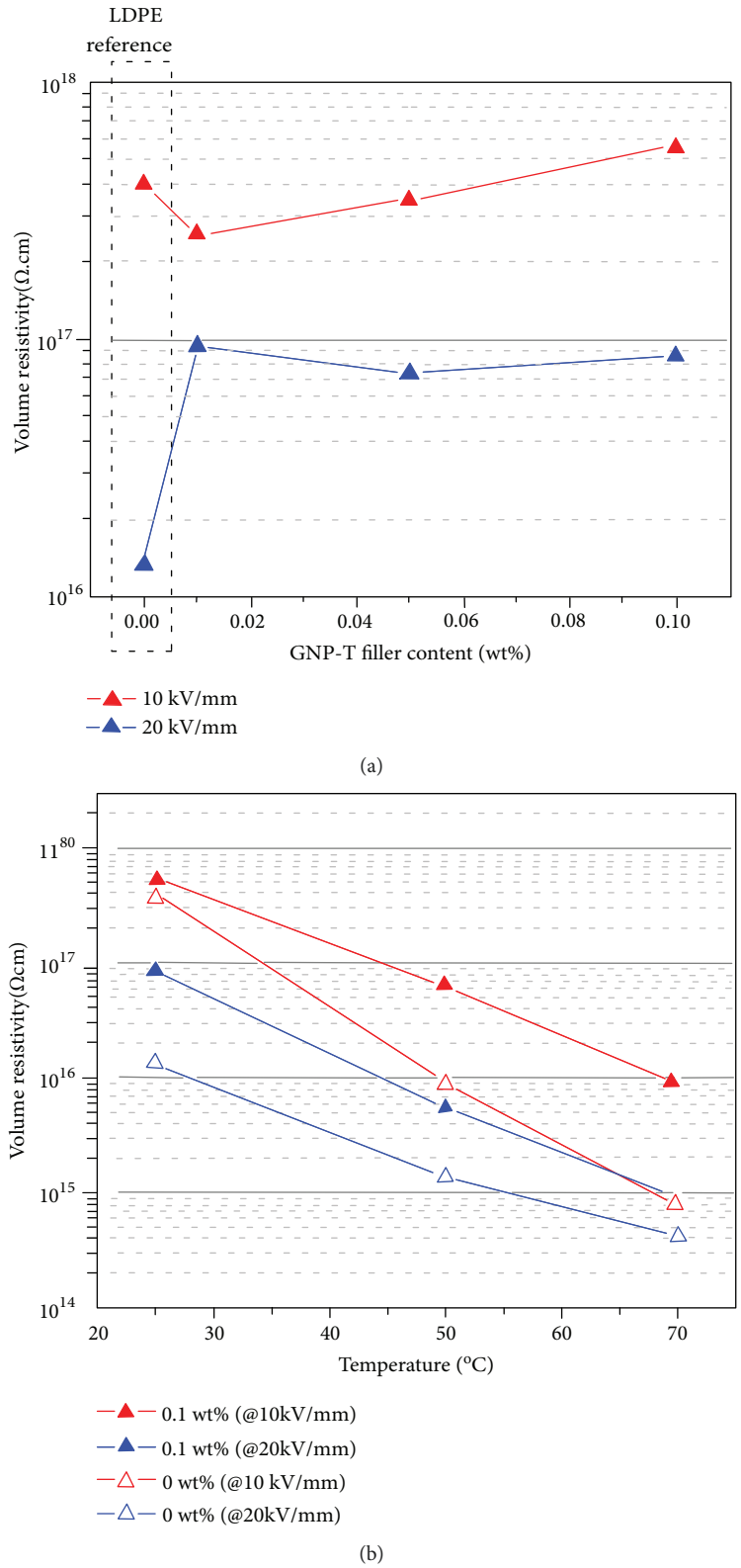

Figure 8: (a) DC volume resistivity of LDPE/GNP-T nanocomposites as a function of GNP-T filler content under constant electric fields of 10 kV/mm and 20 kV/mm at room temperature. (b) DC volume resistivity of LDPE/GNP-T nanocomposites with 0 wt% and 0.1 wt% filler contents measured at various temperatures (25, 50, and 70°C) and electric field (10, 20 kV/mm) conditions.

volume resistivity tended to decrease significantly more than that of the LDPE/GNP-T nanocomposite, resulting in poor insulation characteristics.

4. Conclusions

We demonstrated the hydrophobic surface modification of GNP fillers, via defect-healing process, and an LDPE/GNP-T insulating nanocomposite that can suppress the accumulation of space charges formed in the insulating layer of an HVDC power cable. Through the defect healing via high-temperature heat treatment, pristine GNP fillers with ~13% oxygen content were readily reduced and changed to the hydrophobic surfaces similar to those of an LDPE matrix. Compared to the LDPE/pristine GNP nanocomposite, the LDPE/GNP-T nanocomposite exhibited a well-dispersed filler state corresponding to 33% dispersion enhancement, without severe filler aggregation, when thickness-normalized adsor ption-based Beer-Lambert's law was applied. The effectively dispersed LDPE/GNP-T nanocomposite with 0.1 wt% filler content showed an insulating volume resistivity of 5.5×10^{17} $\Omega \cdot$ cm at the measuring conditions of 10 kV/mm and 25°C. Packet-like space charges were successfully suppressed by the 0.1 wt% GNP-T fillers, which acted as trapping sites; the nanocomposite presented an FEF value of 1.04. This is attributed to the fact that large amounts of deep carrier traps, introduced by well-dispersed dielectric GNP-T fillers, interact with the original trapping sites in LDPE matrix and result in a dramatic increase of deep trap density in LDPE/GNP-T nanocomposite. It is anticipated that our simple approach for the fabrication of polyethylene/GNP-T nanocomposite-based insulating materials promises to raise the upper voltage limit of today's underground/submarine cables.

Data Availability

The data used to support the findings of this study are available from the corresponding author upon request.

Conflicts of Interest

The authors declare that there are no conflicts of interest regarding the publication of this paper.

Acknowledgments

This work was supported by the Technology Innovation Program (no. 20171210201080, Development of ±500 kV HVDC XLPE Submarine Cable System (including Land Cable System)), funded by the Ministry of Trade, Industry and Energy (MOTIE, Korea).

Supplementary Materials

Figure S1: detailed data on the dispersibility for each nanocomposite sample. Figure S2: detailed data on the maximum enhanced electric field for each nanocomposite sample. *(Supplementary Materials)*

References

[1] U. Astrom, B. Westman, V. Lescale, and G. Asplund, "Power transmission with HVDC at voltages above 600 kV," in *Proceedings of the Inaugural IEEE PES 2005 Conference and Exposition in Africa*, pp. 44–50, Piscataway, NJ, USA, 2005.

[2] A. Gustafsson, M. Saltzer, A. Farkas, H. Ghorbani, T. Quist, and M. Jeroense, "The new 525 kV extruded HVDC cable system," ABB Grid Systems, Technical Paper, ABB, 2014.

[3] P. Bergelin, M. Jeroense, T. Quist, and H. Rapp, "640 kV extruded HVDC cable system," NKT, Technical Paper, NKT, 2017.

[4] B. Müller, W. Arlt, and P. Wasserscheid, "A new concept for the global distribution of solar energy: energy carrying compounds," *Energy & Environmental Science*, vol. 4, no. 10, pp. 4322–4331, 2011.

[5] S. Li, Y. Zhu, D. Min, and G. Chen, "Space charge modulated electrical breakdown," *Scientific Reports*, vol. 6, no. 1, article 32588, 2016.

[6] T. Kato, R. Onozawa, H. Miyake, Y. Tanaka, and T. Takada, "Properties of space charge distributions and conduction current in XLPE and LDPE under DC high electric field," *Electrical Engineering in Japan*, vol. 198, no. 3, pp. 19–26, 2017.

[7] M. G. Andersson, J. Hynynen, M. R. Andersson et al., "Highly insulating polyethylene blends for high-voltage direct-current power cables," *ACS Macro Letters*, vol. 6, no. 2, pp. 78–82, 2017.

[8] G. C. Montanari, G. Mazzanti, F. Palmieri, A. Motori, G. Perego, and S. Serra, "Space-charge trapping and conduction in LDPE, HDPE and XLPE," *Journal of Physics D: Applied Physics*, vol. 34, no. 18, pp. 2902–2911, 2001.

[9] T. L. Hanley, R. P. Burford, R. J. Fleming, and K. W. Barber, "A general review of polymeric insulation for use in HVDC cables," *IEEE Electrical Insulation Magazine*, vol. 19, no. 1, pp. 13–24, 2003.

[10] A. M. Pourrahimi, R. T. Olsson, and M. S. Hedenqvist, "The role of interfaces in polyethylene/metal-oxide nanocomposites for ultrahigh-voltage insulating materials," *Advanced Materials*, vol. 30, no. 4, article 1703624, 2018.

[11] L. K. H. Pallon, A. T. Hoang, A. M. Pourrahimi et al., "The impact of MgO nanoparticle interface in ultra-insulating polyethylene nanocomposites for high voltage DC cables," *Journal of Materials Chemistry A*, vol. 4, no. 22, pp. 8590–8601, 2016.

[12] K. Y. Lau, A. S. Vaughan, G. Chen, I. L. Hosier, and A. F. Holt, "Absorption current behaviour of polyethylene/silica nanocomposites," *Journal of Physics: Conference Series*, vol. 472, article 012003, 2013.

[13] S.-J. Wang, J.-W. Zha, W.-K. Li, and Z. M. Dang, "Distinctive electrical properties in sandwich-structured Al_2O_3/low density polyethylene nanocomposites," *Applied Physics Letters*, vol. 108, no. 9, article 092902, 2016.

[14] Y. Wang, K. Xiao, C. Wang, L. Yang, and F. Wang, "Effect of nanoparticle surface modification and filling concentration on space charge characteristics in TiO_2/XLPE nanocomposites," *Journal of Nanomaterials*, vol. 2016, Article ID 2840410, 10 pages, 2016.

[15] A. M. Pourrahimi, T. A. Hoang, D. Liu et al., "Highly efficient interfaces in nanocomposites based on polyethylene and ZnO nano/hierarchical particles: a novel approach toward ultralow electrical conductivity insulations," *Advanced Materials*, vol. 28, no. 39, pp. 8651–8657, 2016.

[16] Y. Tanaka, Y. Li, T. Takada, and M. Ikeda, "Space charge distribution in low-density polyethylene with charge-injection

suppression layers," *Journal of Physics D: Applied Physics*, vol. 28, no. 6, pp. 1232–1238, 1995.

[17] Z. Li, B. du, C. Han, and H. Xu, "Trap modulated charge carrier transport in polyethylene/graphene nanocomposites," *Scientific Reports*, vol. 7, no. 1, p. 4015, 2017.

[18] E. J. G. Santos and E. Kaxiras, "Electric-field dependence of the effective dielectric constant in graphene," *Nano Letters*, vol. 13, no. 3, pp. 898–902, 2013.

[19] F. Boufayed, G. Teyssèdre, C. Laurent et al., "Models of bipolar charge transport in polyethylene," *Journal of Applied Physics*, vol. 100, no. 10, article 104105, 2006.

[20] T. Takada, Y. Hayase, Y. Tanaka, and T. Okamoto, "Space charge trapping in electrical potential well caused by permanent and induced dipoles for LDPE/MgO nanocomposite," *IEEE Transactions on Dielectrics and Electrical Insulation*, vol. 15, no. 1, pp. 152–160, 2008.

[21] T. Tanaka, M. Kozako, N. Fuse, and Y. Ohki, "Proposal of a multi-core model for polymer nanocomposite dielectrics," *IEEE Transactions on Dielectrics and Electrical Insulation*, vol. 12, no. 4, pp. 669–681, 2005.

[22] Y. Lin, G. J. Ehlert, C. Bukowsky, and H. A. Sodano, "Superhydrophobic functionalized graphene aerogels," *ACS Applied Materials & Interfaces*, vol. 3, no. 7, pp. 2200–2203, 2011.

[23] Z. Lin, Y. Liu, and C.-P. Wong, "Facile fabrication of superhydrophobic octadecylamine-functionalized graphite oxide film," *Langmuir*, vol. 26, no. 20, pp. 16110–16114, 2010.

[24] N. Hirai, R. Minami, K. Shibata, Y. Ohki, M. Okashita, and T. Maeno, "Effect of byproducts of dicumyl peroxide on space charge formation in low-density polyethylene," in *2001 Annual Report Conference on Electrical Insulation and Dielectric Phenomena (Cat. No.01CH37225)*, pp. 478–483, Piscataway, NJ, USA, 2001.

[25] R. Tanaka, N. Takahashi, Y. Nakamura, Y. Hattori, K. Ashizawa, and M. Otsuka, "Verification of the mixing processes of the active pharmaceutical ingredient, excipient and lubricant in a pharmaceutical formulation using a resonant acoustic mixing technology," *RSC Advances*, vol. 6, no. 90, pp. 87049–87057, 2016.

[26] J. S. Park, L. Yu, C. S. Lee, K. Shin, and J. H. Han, "Liquid-phase exfoliation of expanded graphites into graphene nanoplatelets using amphiphilic organic molecules," *Journal of Colloid and Interface Science*, vol. 417, pp. 379–384, 2014.

[27] G. W. Curtzwiler, B. Greenhoe, S. K. Mendon et al., "A rapid quantitative protocol for measuring carbon nanotube degree of dispersion in a waterborne epoxy–amine matrix material," *Journal of Coating Technology and Research*, vol. 14, no. 4, pp. 903–913, 2017.

[28] Z. F. Li, G. H. Luo, W. P. Zhou, F. Wei, R. Xiang, and Y. P. Liu, "The quantitative characterization of the concentration and dispersion of multi-walled carbon nanotubes in suspension by spectrophotometry," *Nanotechnology*, vol. 17, no. 15, pp. 3692–3698, 2006.

[29] T. Maeno, T. Futami, H. Kushibe, T. Takada, and C. M. Cooke, "Measurement of spatial charge distribution in thick dielectrics using the pulsed electroacoustic method," *IEEE Transactions on Electrical Insulation*, vol. 23, no. 3, pp. 433–439, 1988.

[30] C. C. Reddy and T. Ramu, "On the computation of electric field and temperature distribution in HVDC cable insulation," *IEEE Transactions on Dielectrics and Electrical Insulation*, vol. 13, no. 6, pp. 1236–1244, 2006.